structure. In addition, photoelectrochemical cells offer interesting practical prospects with respect to the microfabrication of semiconductor structures and remediation of pollutants from contaminated water sources. A third type of interaction of light with an electrochemical environment is the photogalvanic cell, in which a species dissolved in the electrolyte (or chemisorbed on the electrode surface) undergoes a photochemical process that generates a current that is collected at an electrode. The electrode utilized may be constructed of either a metal or a semiconducting material. Recently semiconducting photogalvanic cells have been shown to offer high efficiency for the conversion of visible optical energy to electricity.

Electrochemiluminescence typically involves the electrochemical generation of species that undergo homogeneous reactions to generate electronically excited dissolved compounds. In certain cases, emission can then be observed as these molecular species relax to the ground state. As such, ECL in some sense represents the opposite process of that observed in a photogalvanic cell.

II. PHOTOELECTROCHEMISTRY—SEMICONDUCTOR/ELECTROLYTE INTERFACES

A. Semiconductor Solid-State Physics

While many of the standard electroanalytical techniques utilized with metal electrodes can be employed to characterize the semiconductor–electrolyte interface, one must be careful not to interpret the semiconductor response in terms of the standard diagnostics employed with metal electrodes. Fundamental to our understanding of the metal–electrolyte interface is the assumption that all potential applied to the back side of a metal electrode will appear at the metal electrode surface. That is, in the case of a metal electrode, a potential drop only appears on the solution side of the interface (i.e., via the electrode double layer and the bulk electrolyte resistance). This is not the case when a semiconductor is employed. If the semiconductor responds in an ideal manner, the potential applied to the back side of the electrode will be dropped across the internal electrode–electrolyte interface. This has two implications: (1) the potential applied to a semiconducting electrode does not control the electrochemistry, and (2) in most cases there exists a "built-in" barrier to charge transfer at the semiconductor–electrolyte interface, so that, electrochemical reversible behavior can never exist. In order to understand the radically different response of a semiconductor to an applied external potential, one must explore the solid-state band structure of the semiconductor. This topic is treated at an introductory level in References 1 and 2. A more complete discussion can be found in References 3, 4, 5, and 6, along with a detailed review of the photoelectrochemical response of a wide variety of inorganic semiconducting materials.

offer interesting practical
miconductor structures and
sources. A third type of in-
nt is the photogalvanic cell,
ıemisorbed on the electrode
generates a current that is
y be constructed of either a
nducting photogalvanic cells
onversion of visible optical

e electrochemical generation
:nerate electronically excited
ın then be observed as these
:h, ECL in some sense rep-
photogalvanic cell.

CONDUCTOR/

hniques utilized with metal
iconductor–electrolyte inter-
conductor response in terms
:trodes. Fundamental to our
the assumption that all po-
ıde will appear at the metal
:trode, a potential drop only
ia the electrode double layer
case when a semiconductor
ideal manner, the potential
dropped across the internal
cations: (1) the potential ap-
ol the electrochemistry, and
charge transfer at the semi-
nical reversible behavior can
ifferent response of a semi-
t explore the solid-state band
d at an introductory level in
can be found in References
hotoelectrochemical response
terials.

Solid-state physics depicts a semiconductor as being energetically composed of a series of closely spaced, low-lying, mainly filled orbitals, known as the valence band, and a series of closely spaced, high-energy, mainly vacant orbitals, the conduction band, separated by a forbidden zone known as the band gap (see Fig. 28.1) [6]. The band gaps of several semiconductors that have been extensively investigated as photoelectrodes are given in Table 28.1. The orbitals within each band are delocalized in nature. Thus, a single crystal of a semiconductor is best described as a single molecule, within traditional chemical nomenclature! The interorbital spacing within a band is so small in energy that orbital to orbital transitions occur by thermal activation. Thus, the primary optical characteristics of a semiconductor (including its color) are established by the energy required to promote electrons across the band gap, from the valence band to the conduction band.

In addition to energy, the semiconductor band gap is characterized by whether or not transfer of an electron from the valence band to the conduction band involves changing the angular momentum of the electron. Since photons do not have angular momentum, they can only carry out transitions in which the electron angular momentum is conserved. These are known as direct transitions. Momentum-changing transitions are quantum-mechanically forbidden and are termed indirect (see Table 28.1). These transitions come about by coupling

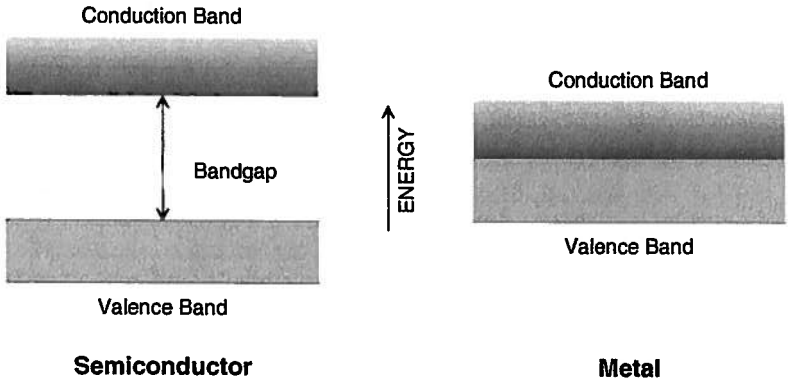

Figure 28.1 The electronic structure of a solid can be described in terms of a band model in which bonding electrons are primarily found in a low-energy valence band, while conduction is typically associated with antibonding or nonbonding high-energy orbitals known as the conduction band. In the case of a semiconductor (left), these two bands are separated by a quantum-mechanical forbidden zone, the band gap. Excitation of electrons from the valence band to the conduction band gives rise to the bulk optical and electronic properties of the semiconductor. In the case of a metal (right), the conduction band and valence band overlap, giving rise to a continuum of states.

Table 28.1 Bandgaps of Common Semiconductors

Semiconductor	Bandgap[a] (eV) (transition type)[b]	Onset wavelength[c] (nm)	Bulk color	Dopant type
Si	1.11 (I)	1100	Black	p or n
InP	1.28 (D)	960	Black	p or n
GaAs	1.35 (D)	915	Black	p or n
CdTe	1.50 (D)	820	Black	p or n
CdSe	1.74 (D)	710	Black	n only
α-Fe_2O_3	2.2 (I)	560	Orange-red	primarily n
GaP	2.24 (I)	550	Orange	p or n
CdS	2.4 (D)	515	Yellow	n only
TiO_2	3.0 (D)	412	Pale yellow/ white	n only
$SrTiO_3$	3.2 (D)	386	White	n only
ZnO	3.2 (I)	386	White	n only
SnO_2	3.6 (D)	340	White	n only

[a]At 300 K.
[b]Transitions that conserve momentum are direct transitions (D); those that involve a change in momentum are indirect transitions (I).
[c]Absorption edge of the bandgap transition.

the absorption of a photon with a phonon (a quantum of solid-state lattice vibration). The net effect is that direct semiconductor transitions give rise to extreme absorptivity very close to the band gap energy, while indirect transitions are associated with a mild increase in absorptivity as one moves to energies greater than the band gap energy.

In general, whether an electrode is a metal or a semiconductor, to sustain a current, electrons must populate the conduction band levels, since these empty delocalized orbitals are needed to allow the electron to be physically transported through space (i.e., from orbital to orbital). In the case of a metal, the band gap is zero; therefore, the valence band and conduction band orbitals overlap (see Fig. 28.1). Thermal excitation of electrons from the valence band to the conduction band orbitals provides for a conductivity pathway. The relatively large band gap of a semiconductor, however, precludes thermal population of the conduction band by valence band electrons. However, optical excitation of the semiconductor with photons of energy greater than or equal to the band gap energy can be employed to produce conduction. Excitation of an electron generates not only an excited conduction band electron but also an empty orbital in the valence band. This empty orbital can undergo a self-exchange process with a filled valence band orbital to effectively "move" the empty orbital through the

Bulk color	Dopant type
Black	p or n
Black	p or n
Black	p or n
Black	p or n
Black	n only
Orange-red	primarily n
Orange	p or n
Yellow	n only
Pale yellow/ white	n only
White	n only
White	n only
White	n only

)); those that involve a change in

tum of solid-state lattice vi-
:tor transitions give rise to
ıergy, while indirect transi-
:ivity as one moves to ener-

a semiconductor, to sustain
nd levels, since these empty
to be physically transported
: case of a metal, the band
ıction band orbitals overlap
om the valence band to the
ity pathway. The relatively
ludes thermal population of
wever, optical excitation of
ıan or equal to the band gap
:citation of an electron gen-
n but also an empty orbital
ı self-exchange process with
ıe empty orbital through the

semiconductor lattice. The "movement" of an empty photoexcited orbital is physically equivalent to the motion of a positively charged particle through a semiconductor lattice. These empty orbitals are referred to as holes (h^+). Thus, a photoinduced current in a semiconductor can be thought of as a flow of conduction band electrons in one direction and an opposing flow of valence band holes. Holes can be given pseudoattributes similar to the properties of electrons, such as charge, mass, velocity, etc.

Simple promotion of electrons across the semiconductor band gap is insufficient to generate a photocurrent, since nonradiative relaxation of excited electrons to the ground state is quite facile in the solid state. This deactivation pathway can be overcome by carrying out a thermal charge-transfer reaction between the semiconductor and a second phase to generate a charge separating electric field at the semiconductor surface (prior to photoexcitation). This interfacial electric field can be used to spatially separate photoinduced electron–hole pairs, thereby preventing their nonradiative recombination. The necessary interfacial electric field can be developed by placing the semiconductor surface in intimate contact with any medium having a free energy different from that of the semiconductor. From an electrochemical point of view, the most interesting contacting phase is an electrolyte.

B. The Ideal Semiconductor-Electrolyte Interface

As shown in Figure 28.2, the contacting of a semiconductor surface by an electrolyte containing an electroactive species having a well-defined redox potential causes (in the dark) the transfer of a limited number of electrons between the semiconductor and the electrolyte. This brings the free energy difference between the semiconductor (the semiconductor's Fermi level) and the electrolyte (the redox potential) to zero, establishing equilibrium. The direction of electron flow during this process will depend on the relative values of the Fermi level and the redox potential. In theory, both the free energy of the semiconductor and the free energy of the electrolyte should change in order to establish the equilibrium condition. However, since there exists a tremendous excess of charge carriers in the electrolyte (i.e., the number of electroactive molecules) compared to the number of charge carriers in the semiconductor, the redox potential of the electrolyte is virtually unaffected by this process. Rather, the semiconductor Fermi level shifts to the electrolyte redox potential.

In order to understand this process, the nature of the Fermi level must be considered. Within the nomenclature of physics, the Fermi level is defined as the energy at which there is a 50% probability of finding an electron in a metal—what a chemist would call the highest filled molecular orbital (i.e., the top of the valence band). In an *intrinsic* semiconductor, a material having a completely filled valence band and a completely empty conduction band, this energy level

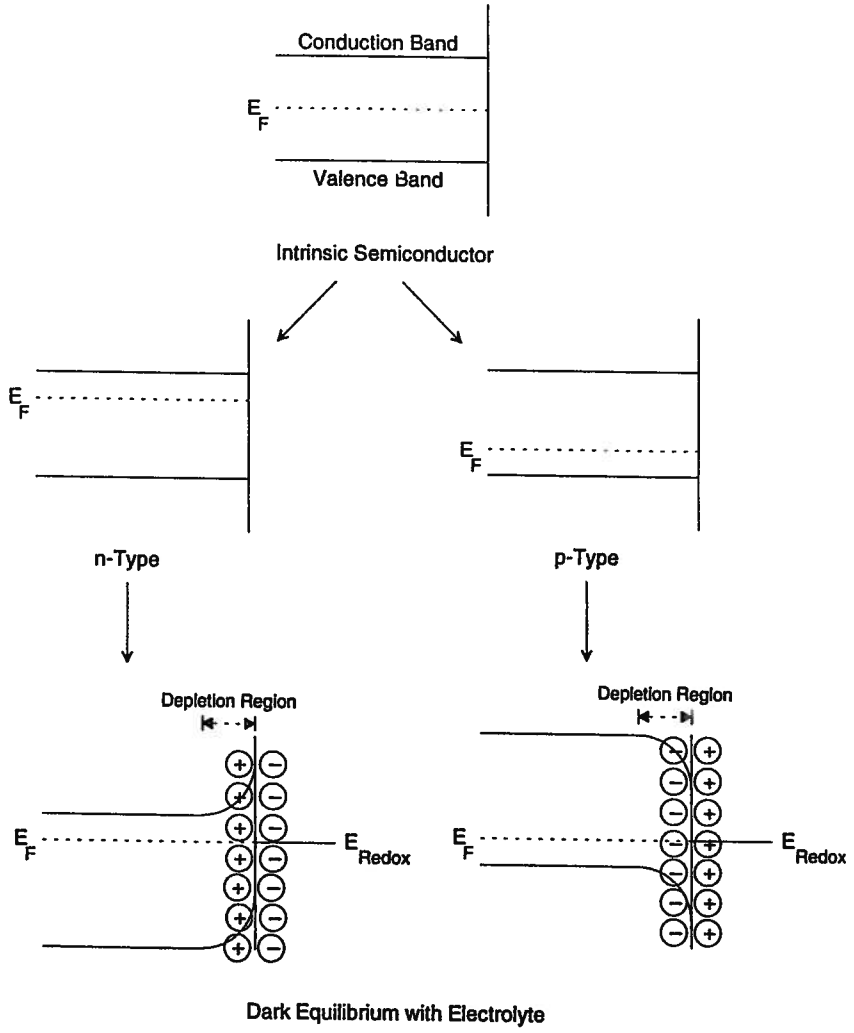

Figure 28.2 An intrinsic semiconductor (top) has a Fermi level that lies in the band gap halfway between the conduction and valence bands. Doping the semiconductor n-type adds electrons to the conduction band, causing the Fermi level to shift higher in energy to a position just below the conduction band edge. Doping a semiconductor p-type adds holes to the valence band, lowering the free energy of the semiconductor and moving the Fermi level to slightly above the valence band edge. In either case, if the semiconductor is contacted with an electrolyte, a dark charge-transfer reaction occurs to bring the semiconductor–electrolyte interface into equilibrium. This establishes a depletion region and related electric field at the semiconductor interface. The band edges in the depletion region bend due to the electric field. In the case of an n-type material, the field is established such as to propel holes in the semiconductor to the interface, while a p-type material yields band bending that causes electrons to move through the interface.

mathematically lies at the center of the bandgap (Fig. 28.2). Of course, no electrons can be found at this energy, since no orbitals exist there. Thus, while retaining its thermodynamic meaning in a semiconductor, the physical picture of the Fermi level is lost. However, using Equation 28.1 the physical significance of the Fermi level can be understood as a solid-state analog of an electrolyte's redox potential,

$$\Delta G = -nFE_F \tag{28.1}$$

where n, the stoichiometric number of electrons, is set equal to 1, F is Faraday's constant, and E_F is the Fermi level. As such, it is appropriate to equate redox potentials and Fermi levels. The Fermi level of a given semiconductor can be adjusted by adding dopants to the semiconductor lattice. These dopants either donate or accept charge (depending on electronegativity). Typical dopant concentrations are very low, generating from 10^{17} to 10^{19} charges per cubic centimeter. If a dopant that is less electronegative than the semiconductor is employed, a small population of high-energy electrons will be added to the semiconductor (conduction band) and the Fermi level will lie close to the conduction band edge (in the band gap). Such semiconductors are known as *n-type*. The electrons in such materials are referred to as the *majority carriers*, while holes are the *minority carriers*. When placed in contact with an electrolyte, electrons typically move from the n-type semiconductor to the solution to establish the equilibrium condition. On the other hand, addition of a highly electronegative dopant to the semiconductor will withdraw electrons from the semiconductor valence band, shifting the Fermi level to an energetic position near the valence band edge (see Fig. 28.2) and making holes the majority carrier. In this case, the semiconductor is referred to as *p-type*, and establishing an electron-transfer equilibrium typically involves moving charge from the electrolyte to the p-type semiconductor. In either case, an electric field, known as the *space charge* or *depletion region*, is established at the semiconductor interface due to a deficiency of majority carriers (Fig. 28.2). This layer typically penetrates 100–10,000 Å into the semiconductor.

At the n-type interface, the electric field generated causes photogenerated conduction band electrons to move into the bulk of the semiconductor, to the back metal contact, and into the external circuit. The valence band holes access the semiconductor interface due to the influence of the interfacial electric field (Fig. 28.2). Thus, redox species can be oxidized by the excited n-type semiconductor. These materials act as photoanodes. On the other hand, the electric field in a p-type material is reversed in potential gradient; therefore, excited electrons move to the semiconductor surface, while holes move through the semiconductor to the external circuit (Fig. 28.2). These materials are photocathodes. The presence of an electric field at the semiconductor–electrolyte interface is usually depicted by a bending of the band edges as shown in Figure 28.2. Elec-

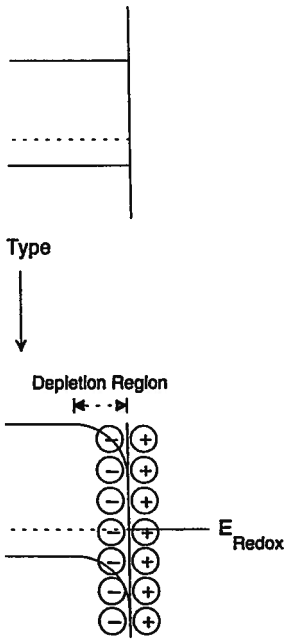

ermi level that lies in the band
Doping the semiconductor n-
rmi level to shift higher in en-
oping a semiconductor p-type
gy of the semiconductor and
id edge. In either case, if the
rge-transfer reaction occurs to
ium. This establishes a deple-
interface. The band edges in
ase of an n-type material, the
iductor to the interface, while
ns to move through the inter-

trons "roll" down the potential gradients indicated by the band bending, while holes "float" up such gradients.

At first glance, band bending appears to suggest that the energetics of the semiconductor surface are fixed while the bulk energetics are changing; the opposite is true. Note that the distance of the band edges with respect to the Fermi level, which is the thermodynamic reference point, is invariant in the bulk of the semiconductor, but changes in the depletion region. Thus, the energetics of the semiconductor are only perturbed in the near-surface region, as is expected for an interfacial charge-transfer reaction involving a relatively insulating material. In order to obtain efficient electron–hole separation, the photoexcited charge carriers must reside in the space charge region. This can occur via two processes: the excited carriers may be generated in the space charge region if a photon is absorbed in this spatial area, or electron–hole pairs may be generated in the bulk of the semiconductor and diffuse into the space charge region. The latter process is relatively inefficient due to the rapidity of excited-state nonradiative decay. Since the photoelectrochemical cell is a front surface device (i.e., the light-absorbing surface is coincident with the space charge region), most of the excited carriers are generated in the region of high band bending. However, as the optical energies employed are decreased to the minimum energy needed to sustain the band-to-band transition, the absorptivity of the semiconductor decreases and charge carriers can be formed in the semiconductor bulk.

Photoexcitation of the semiconductor is expected to decrease the degree of band bending, since promotion of electrons to the conduction band must raise the free energy moving the Fermi level to more negative potentials on an electrochemical scale. At sufficiently high light intensities, the bands will totally flatten out. Under these conditions, the semiconductor cannot support a photocurrent, due to rapid electron–hole recombination; however, a photopotential can still be measured. As shown in Figure 28.3a, in the case where a semiconductor is immersed in an electrolyte having a well-established redox potential (i.e., both components of the redox couple are present) and a second electrode that is in thermodynamic equilibrium with the redox couple is employed, the observed photovoltage is given by

$$V_{photo} = E_F - E_{Redox} \tag{28.2}$$

This value is maximized when E_F reaches the *flatband potential*. Thus, a plot of incident light intensity versus open-circuit electrode potential is expected to saturate at the flatband potential, thereby allowing identification of this potential. A typical experiment of this sort is shown in Figure 28.3b for an n-CdSe electrode immersed in a ferri/ferrocyanide electrolyte.

For an ideal semiconductor–electrolyte interface, the energetics of the band edges at the semiconductor-electrolyte interface are held constant by boundary

ed by the band bending, while

ggest that the energetics of the
< energetics are changing; the
band edges with respect to the
cc point, is invariant in the bulk
tion region. Thus, the energet-
the near-surface region, as is
ion involving a relatively insu-
ron–hole separation, the photo-
charge region. This can occur
generated in the space charge
rea, or electron–hole pairs may
nd diffuse into the space charge
it due to the rapidity of excited-
chemical cell is a front surface
incident with the space charge
ated in the region of high band
loyed are decreased to the mini-
d transition, the absorptivity of
s can be formed in the semicon-

pected to decrease the degree of
the conduction band must raise
e negative potentials on an elec-
tensities, the bands will totally
nductor cannot support a photo-
tion; however, a photopotential
3a, in the case where a semicon-
well-established redox potential
present) and a second electrode
redox couple is employed, the

(28.2)

flatband potential. Thus, a plot
electrode potential is expected to
wing identification of this poten-
n in Figure 28.3b for an n-CdSe
ctrolyte.
erface, the energetics of the band
e are held constant by boundary

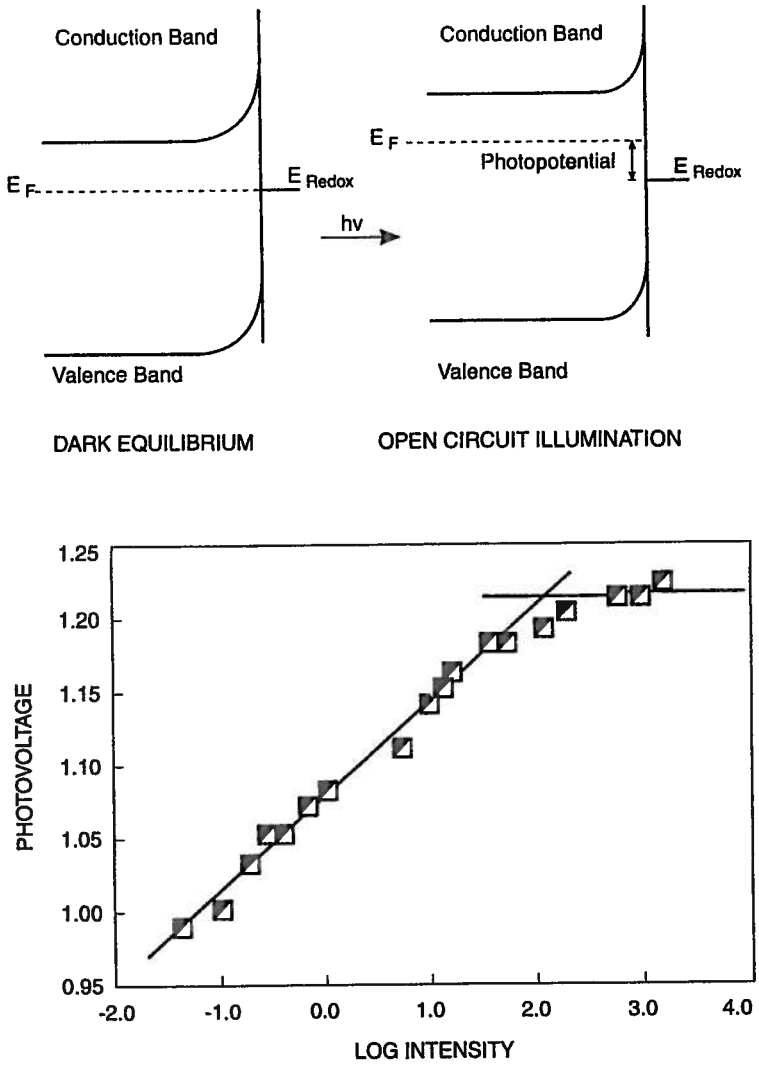

Figure 28.3 The flatband potential of a semiconductor can be established by measuring the photopotential of the semiconductor as a function of illumination intensity. In the dark (left), the semiconductor Fermi level and the redox potential of the electrolyte are equal, providing an equilibrium condition. However, illumination of the semiconductor (right) generates charge carriers that separate the Fermi level and the redox potential. The difference in these two parameters is the observed photovoltage as shown for an n-CdS electrode immersed in a ferri/ferrocyanide electrolyte (bottom). The measured photovoltage is observed to saturate at the flatband potential. In this case, a value of –0.2 V vs. SCE is obtained. Note that the photovoltage response yields a linear functionality at low light intensity with saturation behavior occurring as the flatband potential is approached.

constraints. Additionally, the position of the band edges in the semiconductor bulk is related to the Fermi level by Equation 28.3, and is only dependent on the fractional dopant concentration of the semiconductor:

$$E_c = E_F + kT \ln\left(\frac{n}{N_c}\right) \tag{28.3}$$

where E_c is the energy of the conduction band edge, n is the concentration of donor states per cubic centimeter, and N_c is the density of states in the semiconductor ($N_c \approx 10^{20}$ cm^3). Thus, from the measured flatband potential and a knowledge of the semiconductor band-gap energy, the energetic position of the band edges at the semiconductor surface can be determined. The band-gap energy can be obtained by photoaction spectroscopy. This technique involves monitoring the photopotential or photocurrent of a photoelectrochemical cell as a function of excitation wavelength. The onset of photocurrent (potential) is taken as the band gap. Using the data provided in Figure 28.3 ($E_F = -1.2$ V vs. SCE) and the observed band gap of 1.7 eV, it can be seen that for the n-CdSe/$[Fe(CN)_6]^{4-/3-}$ cell the conduction band edge is at −1.3 V vs. SCE (based on Eq. 28.3, assuming $n \approx 10^{18}$ cm^3), and the valence band edge lies at +0.4 V vs. SCE.

In addition to the use of open-circuit photopotentials, the variation in interfacial capacitance with electrode potential can be utilized to determine the flatband potential as well as the semiconductor dopant concentration. A discussion of the capacitance-potential response of the semiconductor–electrolyte interface is beyond the scope of this text. The reader is referred to Reference 7 for a more complete discussion of this subject.

The position of a semiconductor's Fermi level is sensitive not only to dopant concentration and illumination intensity but also to application of an external potential, as is the case for a metal electrode. Note, however, that although shifting the Fermi level varies the energy of the highest filled metal orbital, and thus the energy at which electrons or holes react at the metal–electrolyte interface, varying the potential of an ideal semiconductor only affects the energy of the Fermi level, and through that the degree of band bending. The extent of band bending determines the efficiency of photoinduced electron–hole separations, it does not affect the energy of the band edges at the semiconductor surface. Under ideal conditions, electrons and holes only react at the energy of the band edge, since nonradiative transfer from an orbital high in the band to the band edge occurs on a rapid time scale. Thus, the oxidizing energetics of an ideal, illuminated n-type semiconductor or the reducing potential of an ideal, illuminated p-type semiconductor is totally determined by the fixed interfacial band edge positions and independent of the electrode potential.

From this discussion, it can be seen that while control over semiconductor potential does not provide control over the interfacial energetics, it does allow one to control the efficiency with which electron-hole pairs are allowed to recombine or alternatively undergo interfacial charge transfer. This process is usually discussed in terms of a quantum yield for electron flow, Φ_e, as defined in

$$\Phi_e = \left(\frac{\text{i/F}}{\text{incident photons/s}} \right) \tag{28.4}$$

where i is the current (hence i/F = moles of electrons in the external circuit per second). Unlike the normal definition of quantum yield, the present definition does not consider photons absorbed; rather, photons incident on the photoelectrochemical cell are monitored. As such, cell reflectivity is viewed as an inherent inefficiency. A given photoelectrochemical cell does not have a single quantum yield that characterizes it. All cells will produce $\Phi_e = 0$ at the flatband potential, with Φ_e rising to a maximum as band bending increases. This effect typically saturates ~300 mV past the flatband potential, at which point the cell current is maximized. The exact potential of Φ_e^{max} depends on the detailed kinetics of interfacial charge transfer, in terms of both electron–hole dynamics within the semiconductor and the classic electrochemical dynamics of heterogeneous charge transfer.

As illustrated in Figure 28.4 for an n-type semiconductor, the dynamics of semiconductor heterogeneous charge-transfer processes are most easily ascertained experimentally by observation of the dark and illuminated steady-state current-potential response of the semiconductor. This voltammetric experiment is typically carried out with a potential scan rate of ~10 mV/s generating conditions similar to those found in a solid electrode polarography experiment. At the flatband potential (Region II), electron–hole pairs cannot be separated and thus no current flows independent of illumination. Moving the electrode potential positive of this point (Region III) introduces band bending. In the dark, this establishes a barrier to charge transfer. The electrode is blocking with respect to anodic current. However, illumination of the electrode under these conditions generates valence band holes that are accelerated through the semiconductor interface by the space charge field. As the band bending is increased, the observed anodic current increases, until additional band bending does not improve charge separation efficiencies and current saturation is observed. If one returns to the flatband potential and now scans the electrode potential in the negative direction, into Region I, the bands are forced to invert, generating a majority carrier *accumulation layer* in the space charge region. Under these conditions, an excess of electrons exists in the interfacial region of an n-type semiconductor (an enrichment of holes would occur in a p-type material). Note that the

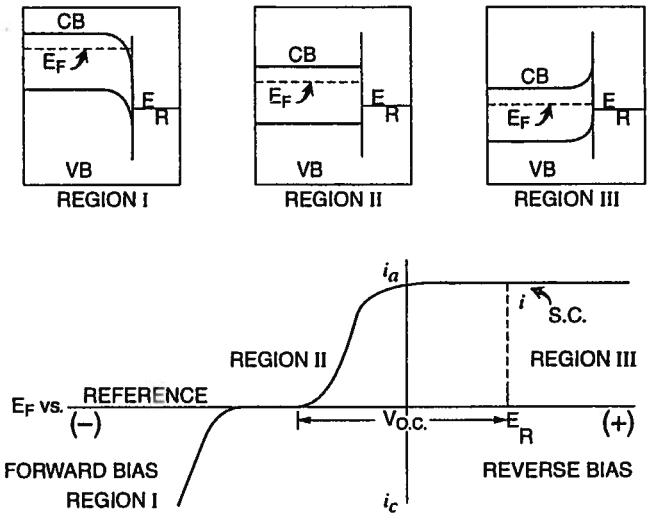

Figure 28.4 The current–potential response of an n-type semiconductor can be divided into three regions. In region I, an accumulation layer exists which allows electrons to be injected into the electrolyte. Thus, the electrode behaves like a dark cathode. In region II, the flatband potential for the electrode is encountered and the electrode is blocking with respect to interfacial charge transfer. In region III, a depletion layer exists. In the dark, the electrode is blocking with respect to charge transfer; however, illumination of the electrode allows valence band holes to be injected into the electrolyte. Thus, the electrode acts as a photoanode. The maximum open-circuit photopotential of an electrode can be obtained from the current–potential curve by noting the potential between photocurrent onset and the redox potential of the electrolyte. The short-circuit photocurrent for the cell is given when the electrode potential is equal to the redox potential of the electrolyte. The fill factor of the cell can be computed based on the percentage of the box defined by the open-circuit photovoltage and the short-circuit current filled by the actual current–voltage curve.

Fermi level under these conditions lies above the conduction band edge in the accumulation region. The conduction band orbitals that fall below the Fermi level are filled with electrons (in the dark). In addition, the direction of band bending causes these electrons to move toward the semiconductor–electrolyte interface. If a reducible electroactive species is present in the electrolyte with a potential positive of the highest filled conduction band orbital, a cathodic current will flow. The mechanism of current flow is similar to that observed at a metal electrode in that moving the Fermi level more negative causes higher energy orbitals to be populated. Thus, n-type semiconductors are not only photoanodes, but dark cathodes. Similar reasoning leads to the conclusion that p-type materials behave as photocathodes and dark anodes.

The current-potential response of a p-type material, p-GaP, is shown in Figure 28.5. A 1 *M* HCl electrolyte has been employed. This electrode acts as an anode at sufficiently positive potentials in the dark (not shown). As expected, the electrode is totally blocking in the dark, at negative potentials indicative of the formation of a depletion layer. The flatband potential for this cell is measured to be about –0.2 V vs. SCE. Under illumination at potentials negative of this potential, photoexcited conduction band electrons migrate to the electrode surface leading to an observed photocathodic current, associated with the reduction of protons to H_2. The thermodynamic redox potential for this process is –0.24 V vs. SCE, and thus a *thermodynamic underpotential* of 40 mV is obtained. In this case, most of the light energy is consumed in overcoming the activation energy for reduction of protons to hydrogen at the GaP interface. Photogenerated valence band holes move into the electrode bulk and through the external circuit. Increasing the band bending to ~300 mV (E_F = –0.1 V vs. SCE) maximizes the charge separation capability of the electrode leading to saturation of

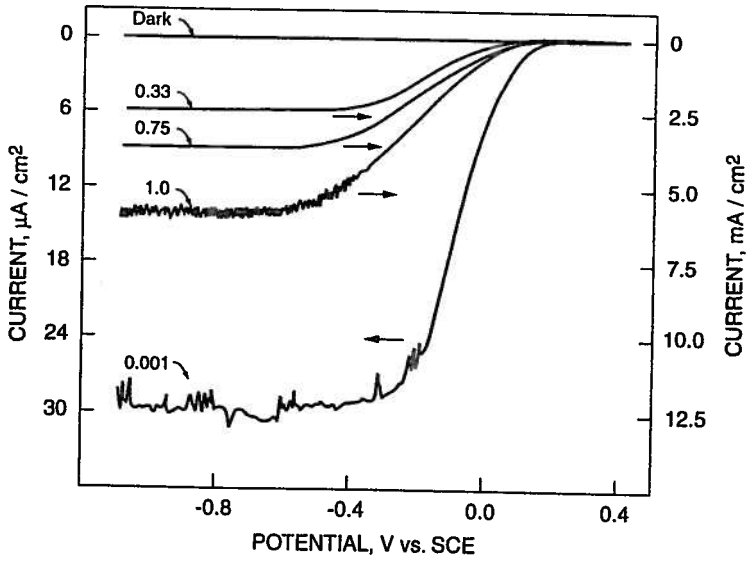

Figure 28.5 Current–potential curves for p-GaP under low- to moderate-intensity illumination; a 1 *M* NaCl (pH = 1) electrolyte is employed. Illumination is from a 200-W high-pressure mercury lamp filtered with neutral density filter. Intensity is relative to the full lamp output. The H_2/H^+ redox potential is –0.3 V vs. SCE in this cell. Thus, this cell yields approximately 400 mV of open-circuit photovoltage. Note that increased illumination increases both the saturation photocurrent and the onset potential. Although the photocurrent is increased at higher light intensities, a calculation of the quantum yield for electron flow indicates that this parameter decreases with increased light intensity.

the photocurrent. Figure 28.5 also demonstrates the effect of light intensity on a potentiostatted photoelectrochemical cell. Under these conditions the semiconductor Fermi level is totally controlled by the potentiostat and is unaffected by the illumination level. The photocurrent is observed to scale with the light intensity. The effect is nonlinear, indicating that Φ_e decreases with increasing light intensity. This may be due to enhanced charge recombination as the effective "concentration" of photoinduced carriers increases, or due to the onset of limitations associated with heterogeneous charge transfer as the carrier concentration is increased.

The photocurrent onset potential is often taken as the flatband potential, since the measurement of the flatband potential is typically only good to ± 100 mV and the onset of photocurrent is often observed with less than 100 mV of band bending. This practice is dangerous, however, since the onset potential is actually the potential at which the dark cathodic current and the photoanodic current are equal. Even though in the case of the p-GaP illustration, the observation of an anodic current and a photocathodic current are separated by several hundred millivolts, in many systems these two currents overlap. In those cases, the relationship between the flatband potential and the onset potential becomes unclear.

In addition to the quantum yield for charge transfer, several other parameters are useful in evaluating a semiconductor's current–potential response. These parameters allow one to quantify the output characteristics of a photoelectrochemical cell as well as the kinetically limiting factors associated with the semiconductor–electrolyte interface. The *fill factor* is a measure of the "squareness" of the current-potential profile and is indicative of the heterogeneous charge-transfer kinetics. In order to define this term, the thermodynamically important positions of the current–potential response must be identified. When the semiconductor Fermi level is equal to the electrolyte redox potential of the electrolyte (and thus the Fermi level of a reversible counterelectrode), no bias voltage is present and a short-circuit condition exists. The cell's open-circuit voltage (i.e., the point at which only a photopotential exists, and no current flows) is obtained as the difference between the short-circuit potential and the photocurrent onset potential. An idealized current–voltage response, devoid of all charge-transfer kinetics, can then be defined as having a photocurrent that jumps from zero to its maximum value instantaneously at the open-circuit potential. A rectangle of fixed area is defined running from the onset potential to the short-circuit potential (see Fig. 28.5). This rectangle represents the active potential region of a photoelectrochemical cell. For a p-type semiconductor at potentials negative of this region, the electrode acts as a dark cathode and thus photoconversion does not occur. Even under optimized conditions, real electrodes do not yield this type of behavior, since the kinetics of

charge separation, recombination, and transport influence the current–voltage response. As a result, a trivially small degree of band bending does not lead to maximum charge separation. Instead, the efficiency with which carriers undergo interfacial charge transfer is observed to increase as the band bending increases. The fill factor is the fraction of the ideal rectangle that actually lies under the current–voltage curve. As such, it represents the impact of carrier kinetics on the thermodynamic response of a photoelectrochemical cell. Improved carrier kinetics lead to an increase in the slope of the current–voltage curve, and an increase in the portion of the thermodynamically defined rectangle that is filled.

In addition to yielding information about semiconductor charge-transfer dynamics, the fill factor parameterizes the efficiency with which the photoelectrochemical cell can be expected to convert optical energy to electricity. The practical value of a photoelectrochemical cell is usually evaluated by its maximum conversion efficiency. The energy conversion efficiency is defined as

$$\eta = \left(\frac{\text{electrical power output}}{\text{optical power input}}\right) - \frac{i \times V_b}{\text{optical watts incident}} \tag{28.5}$$

where V_b is the bias voltage ($= |E_{el} - E_{sc}|$; E_{el} = electrode potential; E_{sc} = short-circuit potential) and i is the current measured at V_b. As the electrode potential is varied from the open-circuit voltage to the short-circuit voltage, V_b decreases while i increases, and thus a plot of η versus potential goes through a maximum. The *maximum power point* is found near the knee of the current–voltage curve.

C. Real (Nonideal) Semiconductor–Electrolyte Interfaces

Photodecomposition Processes

Although several single-crystal, wide-band gap semiconductors provide electrochemical and optical responses close to those expected from the ideal semiconductor–electrolyte model, most semiconducting electrodes do not behave in this manner. The principal and by far overriding deviation from the behavior described in the previous section is photodecomposition of the electrode. This occurs when the semiconductor thermodynamics are such that thermal or photogenerated valence band holes are sufficiently oxidizing to oxidize the semiconductor lattice [8,9]. In this case, kinetics routinely favor semiconductor oxidation over the oxidation of dissolved redox species. For example, irradiation of n-CdX (X = S, Se, or Te) in an aqueous electrolyte gives rise exclusively to semiconductor decomposition products as indicated by

$$CdX \xrightarrow[H_2O]{h\nu} Cd^{2+}_{(aq)} + X^0_{(s)} + XO_y^{n-} \tag{28.6}$$

Likewise, irradiation of an n-Si electrode in an aqueous electrolyte efficiently forms an insulating SiO_x interface [3]. Reductive decomposition of semiconductors is rarely observed, although it has been claimed that certain p-type III–V semiconductors in the phosphide family decompose to form PH_3.

Several successful schemes have been developed to overcome semiconductor photodecomposition. The initial successful approach to this problem was based on the addition of a redox-active species to the electrolyte that could compete with autooxidation of the semiconductor. Thus, addition of ~ 1 M sulfide to an aqueous electrolyte was found to totally suppress the photodecomposition of n-CdS-based cells [11–13]. In this case, oxidation of the sulfide to a polysulfide (Sn^{2-}) is observed. The polysulfide can be reversibly reduced at the dark counterelectrode, giving rise to a cell that undergoes no net chemical change, but is capable of converting optical energy to chemical energy. Similarly, addition of Se^{2-} to n-CdSe-based cells and Te^{2-} to n-CdTe-based cells provides for the stable generation of photocurrent. In these systems a kinetic advantage is achieved by using a reagent which both undergoes a two-electron oxidation and chemically interacts with the electrode interface. The latter conclusion was demonstrated by the observation that the surfaces of n-CdSe photoanodes that were utilized in a S^{2-} containing electrolyte were converted to CdS_xSe_{1-x} [14,15]. It has also been found that chalconide-based electrolytes (i.e., Group 16 anions) are effective at stabilizing certain III–V semiconductor interfaces [16]. In several instances, apparent outer sphere charge-transfer reagents have also been observed to yield some degree of stability to semiconductor interfaces. Most notable is the observation that ferrocyanide stabilizes certain semiconducting interfaces. Although this was initially though to be due to the successful competition of outer sphere kinetics with semiconductor autooxidation, Bocarsly has demonstrated that cyanometalates react with the Cd^{2+} ions generated by the decomposing semiconductor to form an ultrathin (≤ 1 μm) interfacial layer of $[CdFe(CN)_6]^{2-}$ [17]. Stabilization is obtained via a redox reaction between photogenerated holes in the semiconductor and the interfacial cyanometalate layer.

A second approach to semiconductor stabilization is the utilization of an electrolyte in which semiconductor photodecomposition products cannot form. Thus, in the case of n-Si, Lewis has noted that employment of a rigorously anhydrous nonaqueous electrolyte eliminates the possibility of interfacial oxide formation [18]. However, the fact that subnanomolar concentrations of water are sufficient to generate surface oxides makes the application quite difficult. Semiconductors that undergo decomposition to metal ions can likewise be stabilized by using a low-dielectric-constant nonligating electrolyte. Both organic liquids and solid-state ion conductors have been employed for this purpose. Unfortunately, such electrolytes are at best high resistance, and thus observable photocurrents are minimal. However, a hybrid approach in which a nonaqueous

electrolyte (which may contain water) is coupled with a fast outer sphere redox reagent has proved successful in some cases. For example, Wrighton demonstrated that a methanol/TBAP electrolyte containing ferrocene provided n-Si electrodes with a good degree of stability, while allowing for the production of a sizable photocurrent [19].

A more molecular approach to the photocorrosion problem has been to modify the electrode surface chemically with a stabilizing species. The controlled growth of layers of $M_x[CdFe(CN)_6]$ (M = alkali cation) on n-CdX electrodes is an example of this approach. The concept was first introduced by Wrighton, who demonstrated that n-Si electrodes could be stabilized by the covalent attachment of a silylferrocene layer to the electrode surface. This was accomplished by the reaction of a hydrolytically unstable silane such as trichlorosilylferrocene with a single crystal silicon surface, etched to produce a surface containing hydroxyl functionalities. Under these conditions, two types of reactions occurred to tether the reagent to the electrode and to generate a multilayered (polymeric) interfacial structure, illustrated by the following:

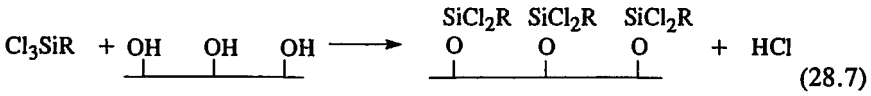

(28.7)

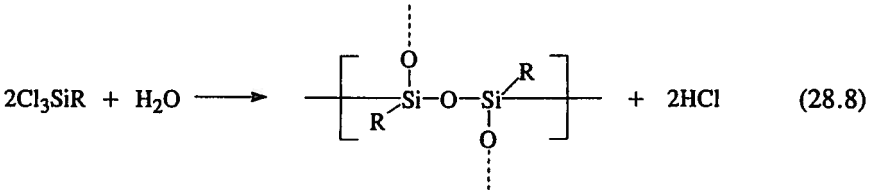

(28.8)

Electrode stabilization is produced by two effects associated with interfacial siloxane formation: The hydrophobic siloxane polymer provides a physical barrier limiting solvation of the electrode decomposition products, and the polymer generates a high effective concentration of the redox moiety (R) at the electrode interface, enhancing the overall interfacial charge-transfer rate. Key to this approach is the presence of a stable surface oxide, since dissolution of this oxide would lead to undercutting of the siloxane interface, physically separating the semiconductor from the protective polymer. Thus, although this approach has been demonstrated to be of utility for the stabilization of Si, Ge, and GaAs electrodes, there is still a small amount of semiconductor decomposition. As indicated earlier for CdX semiconductors in a ferrocyanide electrolyte, one approach to this problem is to utilize one or more of the electrode decomposition products to build the protective overlayer. Using this strategy, transient decomposition processes simply lead to the growth of the protective interface. As

in the case of siloxane-derivatized interfaces, a high concentration of a redox-active species must be present in the interfacial structure to establish a kinetic competition between reversible oxidation of the interfacial material and autooxidation of the semiconductor. In the $CdX/M_x[CdFe(CM)_6]$ systems, the ferrocyanide unit present at ~ 6 *M* serves this purpose [20,21].

One of the key advantages of surface modification, independent of the synthetic approach, is that the stabilized electrode can be operated with a variety of electrolyte solvents and redox couples. For example, the insolubility of ferrocene in water precludes using this reagent to stabilize n-Si in an aqueous electrolyte; however, silylferrocene-derivatized n-Si photoanodes are relatively stable in aqueous electrolytes [22]. In addition to placing stabilizing species on the electrode surface, this same approach can be employed to attach electrocatalysts to the semiconducting electrode. For example, Wrighton's group has placed polymer-bound alkylviologen species on p-Si surfaces [23]. This cationic surface structure could be impregnated with $[PtCl_6]^{2-}$ via an ion-exchange reaction. Once in place, the platinum complex was electroreduced to platinum metal. Upon illumination of the p-Si interface, photogenerated electrons reduced the surface-confined viologen centers. These electrons were then "passed" on to the platinum particles catalyzing the reduction of water to H_2.

Surface and Sub-Band-Gap States

In addition to photodecomposition processes, real electrode behavior is often affected by the fact that there is a variety of localized energy states present on the semiconductor surface. If these states are energetically disposed to communicate with the semiconductor bulk (i.e., their energy is such that charge-transfer overlap with a band can occur), then interfacial charge transfer may proceed through one or more of these states. Orbitals that are spatially localized at the electrode surface (i.e., the molecular orbitals associated with a surface species) are known as *surface states*. In addition to arising from pure lattice species, surface states may be generated by the chemical reactions occurring between the semiconductor surface and the local environment. For example, clean surfaces of silicon have intrinsic surface states due to the fact that the Si atoms on the semiconductor surface are not four-coordinate, as expected for an sp^3-hybridized Si. Thus, surface silicon atoms have nonbonded valence electrons. In addition to the intrinsic surface states, Si readily reacts with oxygen to generate an interfacial layer of SiO_x. This material often contains molecular orbitals of appropriate energy to interact with the Si bands.

The existence of surface states in general can lead to a variety of nonidealities in the output parameters associated with semiconductor-electrolyte junctions. Figure 28.6 provides the current–potential response for a photoelectrochemical cell containing a cadmium ferrocyanide-modified n-CdS electrode in an aqueous ferri/ferrocyanide electrolyte. Although open-circuit and

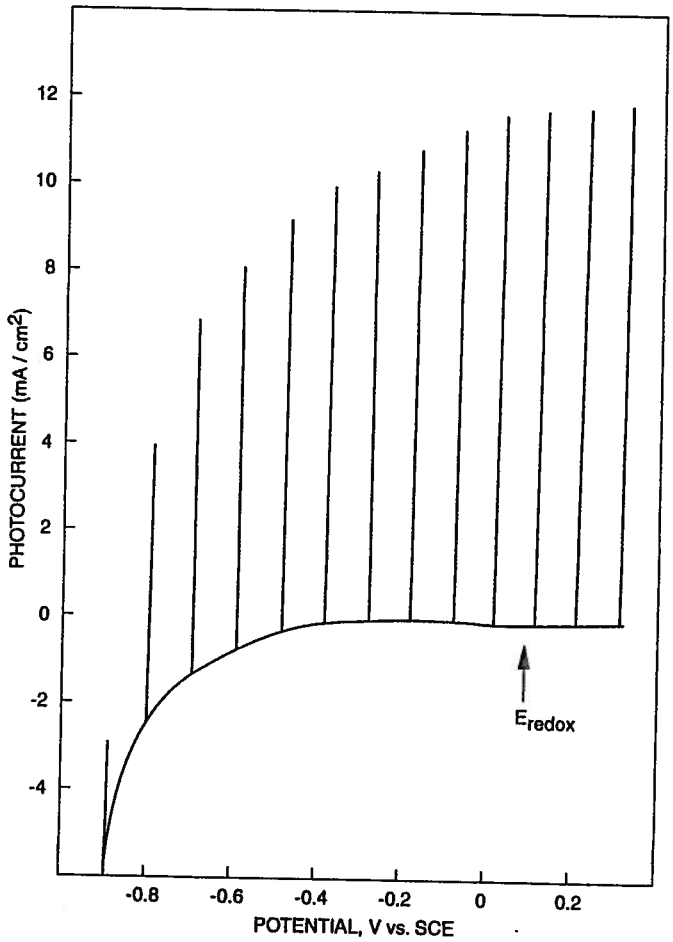

Figure 28.6 The current–potential response of an n-CdS/ferri/ferrocyanide cell under chopped irradiation in (488 nm, 40 mW/cm^2). The ferri/ferrocyanide redox potential is marked in the diagram. Note that even when a dark cathodic current is present (solid line), a photocurrent is observed (spikes).

capacitance measurements indicate that the flatband potential is approximately −1.2 V vs. SCE, the dark current scan clearly shows a cathodic current at potentials significantly positive of this potential [20]. Thus, the n-CdS electrode is able to carry out a dark reduction at potentials where the space charge region is still in depletion (i.e., no accumulation layer exists). This can be accounted for by assuming a set of electrochemically active surface states exists at poten-

tials just positive of (below) the conduction band edge. Such states could shuttle charge from the conduction band to the interface even though a depletion-type band bending exists. Note that the net effect of this situation is that under illumination, the onset potential (the point where cathodic and anodic currents are equal) is nowhere near the flatband potential, and thus the current-potential response cannot be used to estimate the flatband potential.

Since charge carriers can reside in surface states for prolonged time periods, such states often act as electron–hole recombination sites leading to increased cell inefficiency. This is often manifest as a poor fill factor or a low quantum yield for electron flow. In addition to mediating band-to-interface charge-transfer processes, if an extremely high density of surface states is present, they can in theory dominate the observed electrochemistry via a *Fermi level pinning* mechanism. This scenario involves the establishment of an equilibrium between the bulk lattice Fermi level and a Fermi level that represents the average energy of the surface state distribution. The existence of a surface state Fermi level implies a sufficient density of surface states to make a statistical model of these states reasonable. If this criterion is met, then the semiconductor will maintain an internal degree of band bending at the bulk–surface state interface which is independent of the electrolyte employed. A second equilibrium will be established between the surface state population and the electrochemically active solution states. This interaction will appear more or less metallic in nature if a sufficiently broad distribution of surface states is present. The net effect of this interaction will be a photopotential that is invariant with the redox potential of the electrolyte. In terms of a current–potential response, this will give rise to a photocurrent onset that is offset from the redox potential by a fixed amount (the difference between the bulk Fermi level and the surface state Fermi level). Thus, as the nature of the electroactive species is varied, the current–potential response varies. The possibility that this might occur was first discussed by Wrighton and Bard [24]. It has been pointed out that other processes can give rise to identical current–potential properties; thus, whether or not Fermi level pinning is prevalent remains a controversial issue.

Majority Carrier Processes

Phenomenologically similar behavior can be obtained if the redox potential is sufficiently close to the conduction (or valence) band edge to allow for majority carriers to cross the band bending barrier either via a tunneling mechanism or by direct scaling of the barrier. Lewis was the first to demonstrate that the photovoltage of Si photoelectrodes is limited by the kinetics of photogenerated interfacial charge transfer, coupled with the flow of carriers over the semiconductor–electrolyte barrier [18]. This was only observed when the electrolyte couple employed was of an appropriate energy to provide good charge-transfer overlap between the redox species and the semiconductor band states.

ge. Such states could shuttle
/en though a depletion-type
situation is that under illu-
dic and anodic currents are
l thus the current-potential
otential.
es for prolonged time peri-
ination sites leading to in-
a poor fill factor or a low
ediating band-to-interface
ensity of surface states is
ectrochemistry via a *Fermi*
e establishment of an equi-
Fermi level that represents
The existence of a surface
ace states to make a statis-
n is met, then the semicon-
ng at the bulk–surface state
ployed. A second equilib-
opulation and the electro-
will appear more or less
of surface states is present.
ential that is invariant with
current–potential response,
et from the redox potential
Fermi level and the surface
ictive species is varied, the
t this might occur was first
ointed out that other pro-
operties; thus, whether or
roversial issue.

d if the redox potential is
l edge to allow for major-
/ia a tunneling mechanism
st to demonstrate that the
kinetics of photogenerated
f carriers over the semi-
served when the electro-
to provide good charge-
emiconductor band states.

Another mechanism by which charge carriers can overcome the interfacial barrier established by the charge-transfer equilibrium involves the photochemical population of conduction band states that lie above the top of the barrier. Conventional wisdom holds that once populated, rapid nonradiative transfer from such states should lead to the almost immediate transfer of excited electrons to states near the conduction band edge. Thus, thermally *hot electrons* should not exist for a sufficient period of time to allow for interfacial charge transfer. Nozik has proposed, however, that under conditions where the excited electrons are generated near the semiconductor surface, interfacial charge transfer may compete with nonradiative deactivation, allowing hot electrons to move across the semiconductor–electrolyte interface [25]. Recently, Koval has provided experimental evidence showing the production of hot electrons at an illuminated InP interface [26]. The production of hot electrons suggests that reducing potentials well beyond those predicted based on band edge positions can be accessed at the semiconductor interface.

A combination of majority and minority carrier processes has been observed to produce quantum yields in excess of one at both n- and p-type interfaces. In all cases where this has been noted, the redox species employed have been capable of multiple-electron processes. This type of behavior is often seen for the oxidation of carboxylic acids at n-type semiconductors (a two-electron process). It has also been noted for hydrazine oxidation (a four-electron process) and the reduction of hydrogen peroxide.

This phenomenon is known as *current doubling*, although it is not limited to two-electron processes [7]. Using an n-type system as an example, the minimum requirement for current doubling is the generation of a reactive intermediate upon reaction with a valence band hole that can be further oxidized by injection of an electron into the conduction band. For the oxidation of cyanide, the initially generated cyanogen free radical ($CN^- + \text{hole} \rightarrow CN^0$) generates a second redox potential ($CN^0/CN0^-$) that lies well above the n-CdS conduction band edge [113]. Thus, once formed, the cyanogen radical can transfer an electron to an empty conduction band orbital. Hence two charge carriers, a hole in the valence band and an electron in the conduction band, are produced upon absorption of a single photon. Injection of an electron into the conduction band competes with oxidation of CN^0 by a second photogenerated hole. This latter process has a limiting quantum yield of one, since the two-electron oxidation via holes (alone) requires two photons to be absorbed. As a result of these competitive charge-transfer pathways, increased illumination intensity (which produces a higher concentration of interfacial holes) gives rise to a decrease in the observed quantum yield.

D. Polycrystalline Semiconductors

Although most solid-state junctions depend on single-crystal materials to avoid massive electron–hole recombination, photoelectrodes having reasonable effi-

ciency have been produced using less ordered materials. This possibility is due in part to the fact that the photoelectrode is a front junction device. Also important is the role of the electrolyte in avoiding recombination processes. Once the redox-active species has been oxidized (or reduced), it is not subject to further chemistry at the semiconductor interface. As a result, while one observes a lowered quantum yield using electrodes composed of polycrystalline materials, the value is not so low as to be unattractive.

The use of polycrystalline materials is not limited to macroscopic electrodes. Suspended semiconductor particles can also be employed to carry out photoelectrochemical processes [27,28]. In this situation, each semiconducting particle acts like a miniature set of electrodes. If an n-type material is employed, oxidation takes place at illuminated portions of the particle, with reduction occurring in dark regions. As in the case of actual electrodes, kinetic overpotential can dramatically limit charge-transfer processes. Several authors have demonstrated that interfacial charge transfer can be enhanced by placing small islands of electrocatalysts on the particle surface [29–34]. Metal islands (typically Pt) have been utilized both as electron and hole catalysts, while metal oxides such as RuO_2 have proven to be a good oxidation catalyst. One outcome from powder photoelectrochemistry that is not observed in classical photoelectrochemical cells, due to the spatial separation of anode and cathode, is the relative ease with which a material that has been oxidized on an illuminated portion of the particle can be reduced at a dark portion. In cases where fast chemical reactions follow the initial charge-transfer process, this can lead to new product species. To date, this reactivity has been exploited to carry out a variety of sophisticated organic transformations [35].

In addition to providing new synthetic tools, it has been suggested that semiconducting powders may be of use in the natural decontamination of polluted waters. Solar irradiation of natural water supplies that have been treated with semiconducting powders could be used to oxidatively degrade pollutants. For example, the oxidation of cyanide to isocyanate, which decomposes into nitrogen and carbon dioxide, has been demonstrated. The oxidation of halides to atomic halogen and the oxidation of hydroxide to OH^0 has also been observed. These species can be employed as biocides to provide potable water.

E. Dye-Sensitized Semiconducting Electrodes

One solution to the problem of semiconductor photodecomposition is to modify the spectral response of a stable wide-band-gap semiconductor so that solar energy can be efficiently utilized. This can be accomplished by adding to the electrolyte a dye that has absorption features that overlap the solar spectrum. The short excited-state lifetimes of molecular systems limit the distance an excited state can be expected to diffuse prior to nonradiative deactivation. Thus,

unless a photon is absorbed when the dye molecule is near the semiconductor surface, or perhaps adsorbed on the semiconductor, productive charge transfer cannot be expected. As a result, a low concentration of dye must be employed to insure that the bulk of the absorption does not occur in regions of the electrochemical cell that are far from the electrode.

F. Electrolytic Behavior of Adsorbed, Excited Photoreceptors

If a semiconductor electrode such as an n-ZnO crystal is illuminated in the presence of a small amount of dye (e.g., 5×10^{-5} *M* rhodamine B), one can observe an enhanced photocurrent in the anodic region. If illumination is carried out by a tunable, monochromatic source, it is possible to obtain a photocurrent spectrum like that shown in Figure 28.7. In a typical experiment, after removing dissolved O_2 by nitrogen purging, one sets the potential of the semiconductor at a value in the region of limiting photocurrent (ca. +0.5 V vs. SCE) in the absence of dye. This current is simply due to the photoevolution of oxygen as described in Section II.B. If a sensitizing molecule is added to the cell, there is an additional photocurrent whenever illumination occurs at a wavelength absorbed by the sensitizer. In the long-wavelength region, the background photocurrent is often quite small; hence the photocurrent spectrum is essentially identical to the absorption spectrum of the sensitizer.

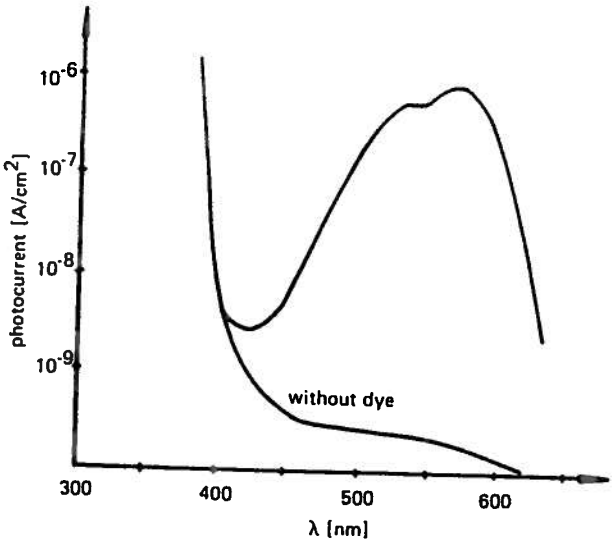

Figure 28.7 Sensitized and unsensitized photocurrent spectrum at a ZnO electrode (doped with Cu). Electrolyte: 1 *M* KCl, pH 2; dye: 10^{-4} *M* rhodamine B. [From Ref. 49, reprinted with permission.]

This phenomenon arises from charge-transfer reactions between the semiconductor and excited dye molecules adsorbed on its surface. If the semiconductor band gap is large compared to the dye's excitation energy, electron transfer between the dye and the electrode may involve the highest normally filled level or the excited level of the dye, but usually not both. One of the dye levels will not be electroactive because it will match some energy in the electrode's band-gap region.

For our specific case, rhodamine B on n-ZnO at +0.5 V vs. SCE, there is no dye electroactivity without illumination, yet an anodic current oxidizes the dye when the light shines. The absence of the dark reaction implies that the highest occupied orbital of the dye is at an energy in the band gap or the valence band. The photocurrent then arises because the absorption raises a dye electron to an excited level that overlaps the conduction band. Thus the net effect is injection of electrons into the conduction band. Hole neutralization cannot explain the observations, because light of smaller energy than the band gap energy will create the effect. Moreover, hole neutralization is fully accounted for by the saturation level of O_2 generation, suggesting the energetic scheme shown in Figure 28.8.

It is interesting to compare this behavior with that expected at a metal electrode. If the Fermi level lies above the highest normally filled dye level, but below the lowest excited level, no dark redox process will occur. If the dye is

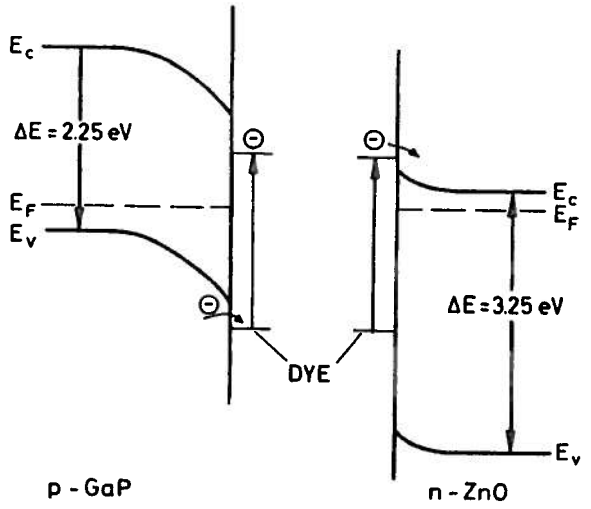

Figure 28.8 Comparison between GaP and ZnO surfaces. [From Ref. 48, reprinted with permission.]

ctions between the semi-
surface. If the semicon-
n energy, electron trans-
highest normally filled
oth. One of the dye lev-
energy in the electrode's

+0.5 V vs. SCE, there
odic current oxidizes the
eaction implies that the
the band gap or the va-
absorption raises a dye
band. Thus the net effect
le neutralization cannot
ergy than the band gap
ation is fully accounted
g the energetic scheme

expected at a metal elec-
lly filled dye level, but
will occur. If the dye is

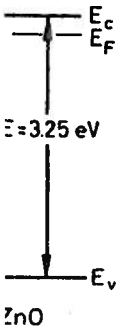

[From Ref. 48, reprinted

then excited, oxidation can occur by removal of an electron from the excited level; but simultaneously, electron transfer from the filled metal levels will reduce the vacancy in the highest normally filled level. The net result is quenching of the excited state by the electrode, but no external current is measured. These consequences follow from the absence of a band gap in the metal.

It has been found that the photosensitized electrochemical process is also influenced by other substances dissolved in solution. For example, the photocurrent from the rhodamine B/n-ZnO system increases when reducing agents such as hydroquinone are added to the system [36]. The hydroquinone serves to restore the adsorbed rhodamine B to its active reduced, ground-state form so that it can undergo repeated absorption acts leading to charge transfer. Several competing mechanisms are now being investigated for this *supersensitization* phenomenon. In contrast, oxygen often reduces (or *desensitizes*) the photocurrent. Typically this is due to quenching of the dye-excited state.

Photosensitized electrochemical reactions using ZnO single crystals with other dyes and solutes have been studied extensively by Gerischer and Tributsch [36,37], Hauffe and co-workers [38], and other groups [39–41]. Photosensitization effects with n-CdS [42,43] and n-TiO_2 [44] are reported to be similar to those with n-ZnO. This type of work has been extended to include covalently bound sensitizers on n-SnO_2 and n-TiO_2 [45–47].

For p-type semiconductors, such as GaAs, GaP, and Cu_2O, sensitized photoelectrochemical behavior is complementary to that seen with n-type material. Electrons are transferred from the valence band to the dye; hence holes are injected into the electrode, and a cathodic current flows. Arguments like those just presented lead to a picture like that presented in Figure 28.8. Results are displayed in Figure 28.9 for p-GaP with *N,N'*-diethylpseudocyanine as sensitizer. In this system, O_2 acts as a supersensitizer. Major studies of p-type electrodes have been carried out by Memming and Gerischer and their coworkers [42,48,49].

Quantum yields for dye-sensitized electrodes are typically quite low, if calculated based on number of photons *incident* on the electrode surface, which is the procedure utilized for reporting quantum yields of pure semiconductor interfaces. However, quantum yields based on the number of photons *absorbed* (the standard approach utilized with molecular systems) are estimated to be about 10%. This value is affected by the actual dye employed, as well as the redox reagents and electrode material [50]. The low quantum yield per incident photon is directly related to the limited number of dye molecules present on an electrode surface. This physical limitation has led some to speculate that dye sensitization will not produce a practically useful photoelectrochemical cell. However, Grätzel has recently announced that TiO_2-based cells utilizing a dye that is a multimetal analog of [$Ru(CN)_2$(2,2'-bipyridine)$_2$] (several ruthenium centers are bridged together via bridging cyanide ligands) yield solar conver-

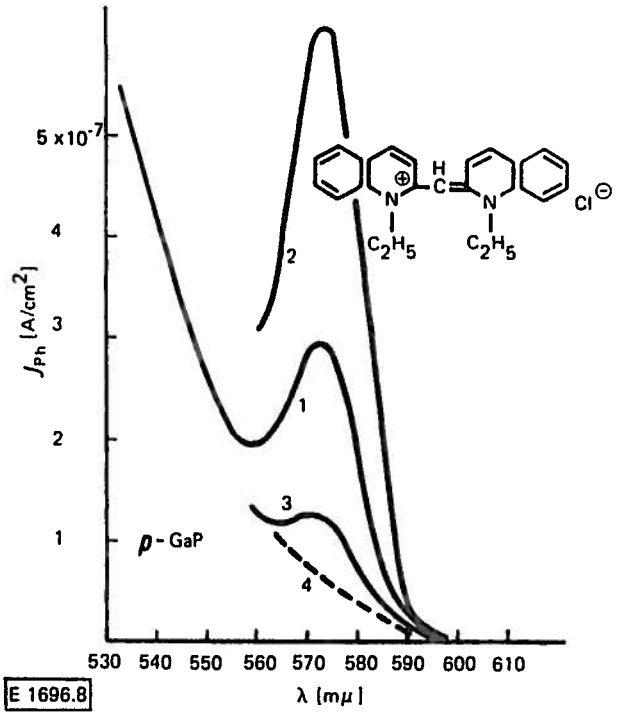

Figure 28.9 Spectral dependence of the photocurrents at a p-type GaP electrode with sensitization by *N,N'*-diethylpseudoisocyanine. [Cathodic photocurrent, electrolyte: 1 *M* KCl + *N,N'*-diethylpseudoisocyanine chloride (1 mL of 10^{-2} *M* ethanol to 10 mL of water).] 1, N_2 flushing; 2, O_2 flushing; 3, addition of piperidine (10^{-2} *M*); 4, trace of the background photocurrent at p-type GaP without dye. [From Ref. 42.]

sion efficiencies on the order of 10%. This level of efficiency is comparable to that obtained from direct semiconductor–electrolyte devices. This impressive efficiency is apparently obtained by utilizing an ultrahigh surface area form of TiO_2. The large surface area allows for the chemisorption of a large quantity of dye. In addition, the roughness of the electrode surface enhances absorption over reflection processes.

Arden and Fromherz [51–53] have reported elegant work involving monolayers of surfactants transferred to electrodes by the Langmuir–Blodgett method. Some results are shown in Figure 28.10. Two separate cationic dyes, thiacyanine (A) and oxacyanine (D), were synthesized with C_{18} alkyl chains, so that they would form oriented monolayers on water–air interfaces. By standard techniques, these were transferred alternatively or in sequence to n-In_2O_3 electrodes, as

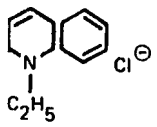

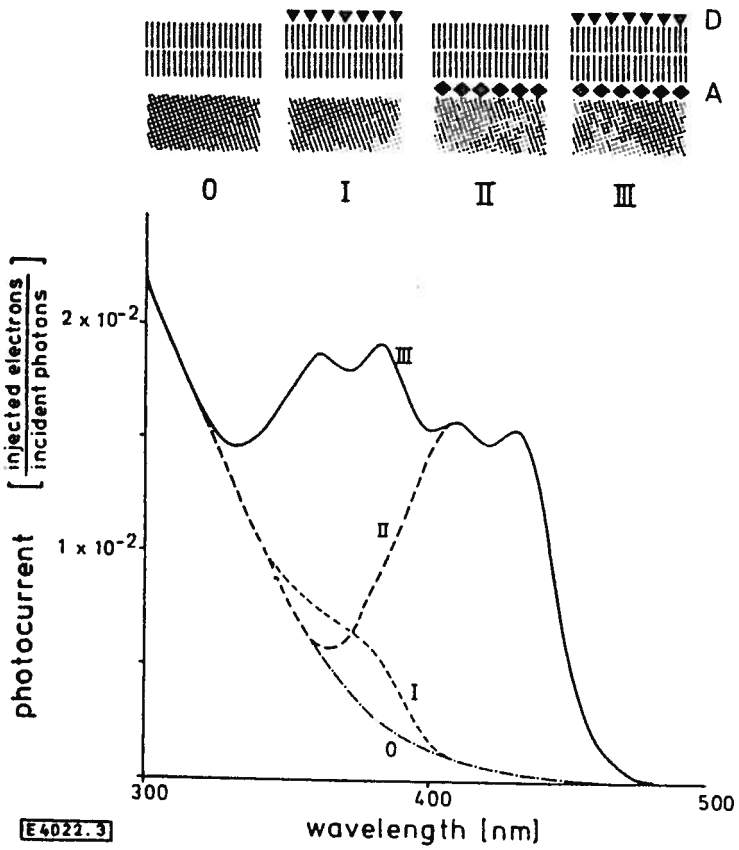

Figure 28.10 Photocurrent per incident photon for various monolayer assemblies on In_2O_3. Configuration 0 is for a bilayer of surfactant molecules without dye deposited on the electrode (represented as the lower shaded area). Configuration I involves the donor dye in the outer layer and configuration II features the acceptor dye in the inner layer. In each of these cases, the remaining layer is made up of a surfactant without dye. Configuration III has both dyes together in the arrangement shown. The electrolyte was 5 m*M* borate buffer of pH 10 with 0.5 *M* allylthiourea as supersensitizer. [From Ref. 53.]

shown at the top of Figure 28.10. The particular orientations shown allow the polar head groups of A and D to interact, respectively, with the polar oxide surface and the aqueous solution, while hydrophobic paraffinic segments interact with each other in the interior of the bilayer. Much optical evidence can be cited for the existence and stability of this type of ordered arrangement [54].

The results in Figure 28.10 show that chromophore A sensitizes photocurrent (curve II), whereas chromophore D has little effect by itself (curve I). The apparent reason for the difference is the remoteness of chromophore A. In the tandem arrangement (III), however, one finds that light absorbed by D (at wavelengths below 380 nm) gives rise to a significant photocurrent. Arden and Fromherz interpret these results to imply that energy absorbed by D is transferred (by the Förster process) to A, which then undergoes charge transfer with the electrode. Without the A underlayer, D cannot sensitize photocurrent; without the D overlayer, A cannot produce significant effects below 380 nm. Luminescence from the D layer can also be observed, and by exploiting it, together with the electrochemical data, Fromherz and Arden have produced some very detailed pictures of interfacial charge-transfer dynamics.

III. PHOTOEMISSION FROM METAL ELECTRODES

Cathodic currents are stimulated by the illumination of metal electrodes [55–59]. These currents are often strongly enhanced by the presence in solution of known electron scavengers such as N_2O and H_3O^+. Research carried out by Barker [59–61], Pleskov [62–64], Delahay [65], and their co-workers indicates rather strongly that the impinging photons eject electrons from the electrode surface. They appear to travel some distance (~ 50 Å) before becoming solvated [55,59,62,65]. If a scavenger is present, the solvated (usually aquated) electrons may react with it irreversibly. For example,

$$e_{aq} + N_2O + H^+ \rightarrow OH^\bullet + N_2 \qquad (28.9)$$

The photoelectrons are then lost permanently from the electrode, and in this case the cathodic current is actually enhanced further by faradaic conversion of $OH^\bullet$ to OH^- [55,59,60]. Without the scavenger, the photocurrent is small, because the photoelectrons return to the electrode, and the net charge transfer is almost zero.

Naturally, one must supply a minimum energy to remove an electron from the electrode; thus there is a *red-limit* wavelength above which photoejection is very improbable [33,34,55]. Since the Fermi level depends on electrode potential, this limit shifts to shorter wavelengths as the potential becomes more positive. Thus there is a threshold potential for photoemission and the emission becomes more probable at more negative potentials [59,62].

Various experimental approaches have been developed for studies of these phenomena [55,59–61,63,65]. Early techniques advanced by Barker's group featured irradiation of a dropping mercury electrod (DMA) by chopped light from low-, medium-, and high-pressure mercury lamps [59]. Pulse polarographic monitoring circuitry synchronized to the light chopper was used for measure-

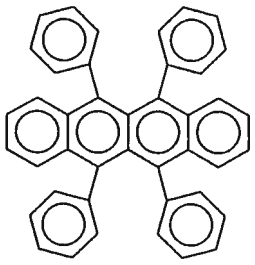

Rubrene

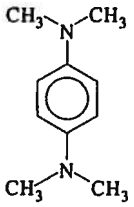

TMPD

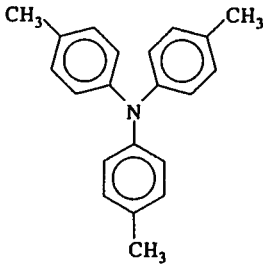

TPTA

REFERENCES

1. S. M. Sze, *Physics of Semiconductor Devices*, Wiley, New York, 1969.
2. C. Kittel, *Introduction to Solid-State Physics*, Wiley, New York, 1971.
3. V. A. Myamlin and Y. V. Pleskov, *Electrochemistry of Semiconductors*, Plenum Press, New York, 1967.
4. S. R. Morrison, *Electrochemistry at Semiconductor and Oxidized Metal Electrodes*, Plenum Press, New York, 1980.
5. H. Gerischer, in *Physical Chemistry: An Advanced Treatise*, Vol. 9A (H. Eyring, D. Henderson, W. Jost, eds.), Academic Press, New York, 1970, Chap. 5.
6. H. O. Finklea, *Semiconductor Electrodes: Studies in Physical and Theoretical Chemistry*, Vol. 55, Elsevier, Amsterdam, 1988.
7. L. M. Peters, *Chem. Rev. 90*:753–769 (1990).
8. A. J. Bard and M. S. Wrighton, *J. Electrochem. Soc. 124*:1706–1710 (1977).
9. H. Gerischer, *J. Electroanal. Chem. 82*:133–143 (1977).
10. R. Williams, *J. Chem. Phys. 32*:1505 (1960).
11. A. B. Ellis, S. W. Kaiser, and M. S. Wrighton, *J. Am. Chem. Soc. 98*:1635 (1976).
12. G. Hodes, J. Manassen, and D. Cahen, *Nature 261*:403 (1976).
13. B. Miller, and A. Heller, *Nature 262*:680 (1976).
14. H. C. Chang, A. Heller, B. Schwartz, S. Menezes, and B. Miller, *Science 196*:1097 (1977).
15. D. Cahen, G. Hodes, and J. Manassen, *J. Electrochem. Soc. 125*:1623 (1978).
16. A. Heller and B. Miller, *Adv. Chem. Ser. 184*:215 (1980).
17. H. D. Rubin, B. D. Humphrey, and A. B. Bocarsly, *Nature 308*:339 (1984).
18. C. M. Gronet, N. S. Lewis, G. Cogan, and J. Gibbons, *Proc. Natl. Acad. Sci. USA 80*:1152 (1983).
19. M. S. Wrighton, A. B. Bocarsly, J. M. Bolts, M. G. Bradley, A. B. Fischer, N. S. Lewis, M. C. Palazzotto, and E. G. Walton, *Adv. Chem. Ser. 184*:269 (1980).
20. H. D. Rubin, D. J. Arent, B. D. Humphrey, and A. B. Bocarsly, *J. Electrochem. Soc. 134*:93 (1987).
21. D. J. Arent, H. D. Rubin, Y. Chen, and A. B. Bocarsly, *J. Electrochem. Soc. 139*:2705–2712 (1992).

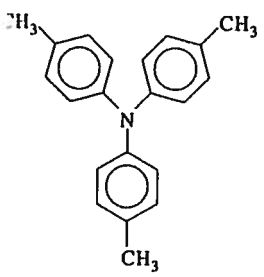

TPTA

New York, 1969.
New York, 1971.
f Semiconductors, Plenum

ınd Oxidized Metal Elec-

ıtise, Vol. 9A (H. Eyring,
York, 1970, Chap. 5.
Physical and Theoretical

124:1706–1710 (1977).
7).

ım. Chem. Soc. 98:1635

3 (1976).

and B. Miller, *Science*

. Soc. 125:1623 (1978).
80).
ature 308:339 (1984).
s, *Proc. Natl. Acad. Sci.*

radley, A. B. Fischer, N.
em. Ser. 184:269 (1980).
Bocarsly, *J. Electrochem.*

ly, *J. Electrochem. Soc.*

22. A. B. Bocarsly, E. G. Walton, and M. S. Wrighton, *J. Am. Chem. Soc. 102*:3390 (1980).
23. D. C. Bookbinder, J. A. Bruce, R. N. Dominey, N. S. Lewis, and M. S. Wrighton, *Proc. Natl. Acad. Sci. USA 77*:6280 (1980).
24. A. J. Bard, A. B. Bocarsly, F.-R. Fan, E. G. Walton, and M. S. Wrighton, *J. Am. Chem. Soc. 102*:3671 (1980).
25. A. J. Nozik, C. A. Parsons, D. J. Dunlavy, B. M. Keyes, and R. K. Ahrenkiel, *Solid State Commun. 75*:297 (1990).
26. C. A. Koval, and P. R. Segar, *J. Phys. Chem. 94*:2033–2039 (1990).
27. A. J. Bard, *Science 207*:139 (1980).
28. A. Heller, *Acc. Chem. Res. 23*:128 (1990).
29. S. N. Frank and A. J. Bard, *J. Phys. Chem. 81*:1484 (1977).
30. T. Fruend and W. P. Gomes, *Catal. Rev. 3*:1 (1969).
31. B. Kraeutler and A. J. Bard, *J. Am. Chem. Soc. 100*:2239 (1978).
32. B. Kraeutler and A. J. Bard, *J. Am. Chem. Soc. 100*:5985 (1978).
33. M. Grätzel, *Faraday Discuss. Chem. Soc. 70*:311 (1980).
34. M. Grätzel, *Acc. Chem. Res. 14*:376 (1981).
35. M. A. Fox, *Acc. Chem. Res. 16*:314 (1983).
36. H. Gerischer and H. Tributsch, *Ber. Bunsen-Ges. Phys. Chem. 72*:437 (1968).
37. H. Tributsch and H. Gerischer, *Ber. Bunsen-Ges. Phys. Chem. 73*:251 (1969); H. Tributsch, *Ber. Bunsen-Ges. Phys. Chem. 73*:582 (1969); H. Tributsch and H. Gerischer, *Ber. Bunsen-Ges. Phys. Chem. 73*:850 (1969); H. Gerischer, M. E. Michel-Beyerle, F. Rebentrost, and H. Tributsch, *Electrochim. Acta 13*:1509; H. Gerischer, *Photochem. Photobiol. 16*:243 (1972).
38. K. Hauffe, H. J. Danzmann, H. Pusch, J. Rauge, and H. Volz, *J. Electrochem. Soc. 117*:993 (1970).
39. H. Tributsch and M. Calvin, *Photochem. Photobiol. 14*:95 (1971).
40. A. Terenin and I. Akimov, *J. Phys. Chem. 69*:730 (1965).
41. W. P. Gomes and F. Cardon, *Ber. Bunsen-Ges. Phys. Chem. 75*:914 (1971).
42. H. Tributsch and H. Gerischer, *Ber. Bunsen-Ges. Phys. Chem. 73*:850 (1969).
43. A. Fujishima, T. Watanabe, O. Tatsuoki, and K. Honda, *Chem. Lett.* 13 (1975).
44. A. Fujishima, E. Hayashitani, and K. Honda, *J. Inst. Ind. Sci.* Univ. Tokyo *(Seisan Kenkyo) 23*:363 (1971).
45. T. Osa and M. Fujihira, *Nature 264*:349 (1976).
46. M. Fujihira, N. Ohishi, and T. Osa, *Nature 268*:226 (1977).
47. M. Fujihira, T. Osa, D. Hursh, and T. Kuwana, *J. Electroanal. Chem. 88*:285 (1978).
48. R. Memming and H. Tributsch, *J. Phys. Chem. 75*:562 (1971).
49. H. Gerischer, *Photochem. Photobiol. 16*:243 (1972).
50. H. Tributsch, *Photochem. Photobiol. 16*:261 (1972).
51. W. Arden and P. Fromherz, *Ber. Bunsen-Ges. Phys. Chem. 82*:868 (1978).
52. W. Arden and P. Fromherz, *J. Electrochem. Soc. 127*:370 (1980).
53. P. Fromherz and W. Arden, *Ber. Bunsen-Ges. Phys. Chem. 84*:1045 (1980).
54. H. Bücher, K. H. Drexhage, M. Fleck, H. Kuhn, D. Möbius, F.P. Schaefer, J. Sondermann, W. Sperling, P. Tillman, and J. Wiegand, *Mol. Cryst. 2*:199 (1967).

55. Yu. Ya. Gurevich, Yu. V. Pleskov, and Z. A. Rotenberg, *Photoelectrochemistry*, Plenum Press, New York, 1978.
56. Yu. V. Pleskov and Z. A. Rotenberg, *Adv. Electrochem. Eng. 11*:1 (1978).
57. M. Heyrovsky and R. G. W. Norrish, *Nature 200*:880 (1963); M. Heyrovsky, *Nature 206*:1356 (1965).
58. H. Berg and H. Schweiss, *Electrochim. Acta 9*:425 (1964).
59. G. C. Barker, A. W. Gardner, and D. C. Sammon, *J. Electrochem. Soc. 113*:1182 (1966).
60. G. C. Barker, *Ber. Bunsen-Ges. Phys. Chem. 75*:728 (1971).
61. G. C. Barker, D. McKeown, M. J. Williams, G. Bottura, and V. Concialini, *Faraday Discuss. Chem. Soc. 56*:41 (1974).
62. Yu. V. Pleskov and Z. A. Rotenberg, *J. Electroanal. Chem. 20*:1 (1969).
63. A. Brodsky and Yu. V. Pleskov, in *Progress in Surface Sciences*, Vol. 2, Part 1 (S. G. Davison, ed.), Pergamon Press, Oxford, 1972.
64. Yu.V. Pleskov, Z. A. Rotenberg, V. V. Eletsky, and V. I. Lakomov, *Faraday Discuss. Chem. Soc. 56*:52 (1974).
65. P. Delahay and V. S. Srinivasan, *J. Phys. Chem. 70*:420 (1966).
66. T. Kuwana, in *Electroanalytical Chemistry*, Vol. 1 (A. J. Bard, ed.), Marcel Dekker, New York, 1966, Chap. 3 and references therein.
67. S. P. Perone and H. D. Drew, in *Analytical Photochemistry and Photochemical Analysis: Solids, Solutions, and Polymers* (J. Fitzgerald, ed.), Marcel Dekker, New York, 1971, Chap. 7 and references therein.
68. H. Berg and H. Schweiss, *Naturwissenschaften 47*:513 (1960).
69. H. Berg, H. Schweiss, E. Stutter, and K. Weller, *J. Electroanal. Chem. 15*:415 (1967), and references therein.
70. G. Porter, in *Techniques of Organic Chemistry*, Vol. 3, Part II (A. Weissberger, ed.), Wiley-Interscience, New York, 1963, Chap. XIX.
71. H. Berg and H. Schweiss, *Nature 191*:1270 (1961).
72. S. P. Perone and J. R. Birk, *Anal. Chem. 38*:1589 (1966).
73. G. L. Kirschner and S. P. Perone, *Anal. Chem. 44*:443 (1972).
74. R. A. Jamieson and S. P. Perone, *J. Phys. Chem. 76*:830 (1972).
75. J. I. H. Patterson and S. P. Perone, *J. Phys. Chem. 77*:2437 (1973).
76. J. I. H. Patterson and S. P. Perone, *Anal. Chem. 44*:1978 (1972).
77. M. Grätzel and A. Henglein, *Ber. Bunsen-Ges. Phys. Chem. 77*:2 (1973); *77*:6 (1973); *77*:11 (1973); *77*:17 (1973).
78. A. Henglein, *Electroanal. Chem. 9*:163 (1976).
79. D. C. Johnson and E. W. Resnick, *Anal. Chem. 44*:637 (1972).
80. J. R. Lubbers, E. W. Resnick, P. R. Gaines, and D. C. Johnson, *Anal. Chem. 46*:865 (1974).
81. W. J. Albery, M. D. Archer, N. J. Field, and A. D. Turner, *Faraday Discuss. Chem. Soc. 56*:28 (1974).
82. A. J. Bard and L. R. Faulkner, *Electrochemical Methods*, Wiley, New York, 1980, Chap. 14.
83. E. A. Chandross, *Trans. N.Y. Acad. Sci., Ser. 2*:32, 571 (1969), and references therein.

84. D. M. Hercules, in *Physical Methods of Organic Chemistry*, Part II (A. Weissberger and B. Rossiter, eds.), Academic Press, New York, 1971, and references therein.
85. A. J. Bard, C. P. Keszthelyi, H. Tachikawa, and N. E. Tokel, in *Chemiluminescence and Bioluminescence* (D. M. Hercules, J. Lee, and M. Cormier, eds.), Plenum Press, New York, 1973, and references contained therein.
86. L. R. Faulkner, *Int. Rev. Sci., Phys. Chem., Ser. 29*:213 (1975).
87. L. R. Faulkner and A. J. Bard, *Electroanal. Chem. 10*:1 (1977).
88. F. Pragst, *Z. Chem. 18*:41 (1978).
89. L. R. Faulkner, *Methods Enzymol. 57*:494 (1978).
90. R. S. Glass and L. R. Faulkner, in *Chemical and Biological Generation of Excited States* (W. Adam and G. Cilento, eds.), Academic Press, New York, 1982, Chap. 6.
91. R. A. Marcus, *Annu. Rev. Phys. Chem. 15*:155 (1964).
92. R. A. Marcus, *J. Chem. Phys. 43*:2654 (1965); *52*:2083 (1970).
93. R. P. Van Duyne and S. F. Fischer, *J. Chem. Phys. 5*:183 (1974).
94. E. A. Mayeda and A. J. Bard, *J. Am. Chem. Soc. 95*:6223 (1973).
95. N. E. Tokel-Takvoryan, R. E. Hemingway, and A. J. Bard, *J. Am. Chem. Soc. 95*:6582 (1973).
96. J. E. Martin, E. J. Hart, A. W. Adamson, H. Gafney, and J. Halpern, *J. Am. Chem. Soc. 94*:9238 (1972).
97. D. M. Hercules and F. E. Lytle, *J. Am. Chem. Soc. 88*:4745 (1966).
98. J. T. Maloy, K. B. Prater, and A. J. Bard, *J. Am. Chem. Soc. 93*:5959 (1971).
99. D. J. Freed and L. R. Faulkner, *J. Am. Chem. Soc. 93*:2097 (1971).
100. C. P. Keszthelyi, N. E. Tokel-Takvoryan, and A. J. Bard, *Anal. Chem. 47*:249 (1975).
101. P. R. Michael and L. R. Faulkner, *Anal. Chem. 48*:1188 (1976).
102. P. R. Michael and L. R. Faulkner, *J. Am. Chem. Soc. 99*:7754 (1977).
103. W. L. Wallace and A. J. Bard, *J. Phys. Chem. 83*:1350 (1979).
104. S. W. Feldberg, *J. Am. Chem. Soc. 88*:390 (1966).
105. S. W. Feldberg, *J. Phys. Chem. 70*:3928 (1966).
106. L. R. Faulkner, *J. Electrochem. Soc. 124*:1724 (1977).
107. J. L. Morris, Jr. and L. R. Faulkner, *J. Electrochem. Soc. 125*:1079 (1978).
108. J. D. Luttmer and A. J. Bard, *J. Phys. Chem. 85*:1155 (1981).
109. R. S. Glass and L. R. Faulkner, *J. Phys. Chem. 85*:1160 (1981).
110. R. S. Glass and L. R. Faulkner, *J. Phys. Chem. 86*:1652 (1982).
111. L. R. Faulkner, H. Tachikawa, and A. J. Bard, *J. Am. Chem. Soc. 94*:691 (1972).
112. R. E. Merrifield, *J. Chem. Phys. 48*:4318 (1968).
113. G. Seshadri, J. K. M. Chun, and A. B. Bocarsly, *Nature, 352*:508 (1991).

Laboratory Techniques in Electroanalytical Chemistry

Second Edition, Revised and Expanded

edited by

Peter T. Kissinger
Purdue University and
Bioanalytical Systems, Inc.
West Lafayette, Indiana

William R. Heineman
University of Cincinnati
Cincinnati, Ohio

Marcel Dekker, Inc. New York • Basel • Hong Kong

QD
115
.L23
1996

Library of Congress Cataloging-in-Publication Data

Laboratory techniques in electroanalytical chemistry / edited by Peter T. Kissinger, William R. Heineman. — 2nd ed., rev. and expanded.
p. cm.
Includes bibliographical references and index.
ISBN 0-8247-9445-1 (hardcover : alk. paper)
1. Electrochemical analysis—Laboratory manuals. I. Kissinger, Peter T. II. Heineman, William R.
QD115.L23 1996
543'.087—dc20 95-46373
CIP

The publisher offers discounts on this book when ordered in bulk quantities. For more information, write to Special Sales/Professional Marketing at the address below.

This book is printed on acid-free paper.

Copyright © 1996 by MARCEL DEKKER, INC. All Rights Reserved.

Neither this book nor any part may be reproduced or transmitted in any form or by any means, electronic or mechanical, including photocopying, microfilming, and recording, or by any information storage and retrieval system, without permission in writing from the publisher.

MARCEL DEKKER, INC.
270 Madison Avenue, New York, New York 10016

Current printing (last digit):
10 9 8 7 6 5 4 3 2 1

PRINTED IN THE UNITED STATES OF AMERICA

The text that had the
chemists between the l
mental Methods in Ele
played a dominant rol
its modern course—b
electrogravimetry of a
developed by Clark in
cal tools. Modern eng
problems in the 1950s
ers revolutionized exp

In the 1960s, mo
chemistry advanced r
chronoamperometry, r
resonance and optical
After a burst of trem
chronopotentiometry v
In the second half of t
electrodes other than r
ered that platinum wa
solvents, and even the
of thin films of metal
solve chemical proble
trodes (1969), surpris
Anodic stripping volta
to compete, for some
ally diminished in imp
little company in Prin
ing differential pulse p
cant op-amp-based el

COLORADO